Digest Journal of Nanomaterials and Biostructures Vol. 16, No. 4, October-December 2021, p.1313-1327

Proposal of new semiconductors spinel oxides Fe_3BO_6 and $Rh_{0.08}Fe_{0.92}BO_6$: ab-initio calculations and prospects for optoelectronic and thermoelectric applications

M. Irfan[a], S. Azam[b*], F. Subhan[c], A. Ur Rahman[b], I. ahmad[c], Z. Abbass, A. Dahshan[d,e], S. S. Ahmad[f], Imran Zada[f], R. Neffati[g,h]

[a] *Department of Physics, Hazara University, Mansehra, Pakistan*

[b] *Pakistan Faculty of Engineering and Applied Sciences, Department of Physics, RIPHAH International University I-14 Campus Islamabad, Pakistan*

[c] *Department of Physics, The Government Post Graduate College Swabi, KP, Pakistan*

[d] *Department of Physics - Faculty of Science - King Khalid University, P.O. Box 9004, Abha, Saudi Arabia.*

[e] *Department of Physics, Faculty of Science, Port Said University, Port Said, Egypt.*

[f] *Department of Physics, University of Swabi, Pakistan*

[g] *Department of Physics, Faculty of Science, King Khalid University; P.O. Box 9004, Abha, Saudi Arabia.*

[h] *Condensed Matter Physics Laboratory, Department of Physics, Faculty of Sciences of Tunis, University El Manar of Tunis, 1060 Tunis, Tunisia*

Transparent conducting oxides (TCOs) are semiconductors gaind much interest due to applications in optoelectronic and tranport properties. Herein, we investigated optoelectronic and tranport properties of Rh doped Fe_3BO_6 compound. The band structure of parent compound for spin up shows insulating nature while other channel is semiconducting nature (4.181 eV Up/2.41 eV Dn).When spinel material doped with Rh^{3+}, the band gap is reduced for both spin channels (2.59 eV (Up)/ 0.59 (Dn), respectively. The optical dispersion exhibits strong absorption in the UV region, for both materials. Reflectivity spectra, for both materials visible-UV indicating good coating materials to reduce solar heating. The transport parameters are computed. It's observed that large ZT value Fe_3BO_6 made this compoud most promisining in thermoelectric applications. The effective masses of species were also analyzed by curve fitting method, results showed that nature of band at 0.69 is changed from direct to indirect for doped compound.

(Received July 1, 2021; Accepted October 19, 2021)

Keywords: DFT, Spinel oxides, Optical properties, Magnetic moment, Thermoelectric properties, Effective masses

1. Introduction

Anhydrous oxyborates is a family of 3d transition metals compounds which exists in various chemical structures and compostions [1-8]. In case of ternary Fe-B-O system ($FeBO_3$ [9], Fe_3BO_6 [10]) Fe(III) borates, Fe_2BO_4[11] and Fe_3BO_5[12] have been investigated extensively from previous years. The chemical formula of three basic groups are $Fe^{2+}Fe^{3+}OBO_3$, $Fe_2^{2+}Fe^{3+}O_2BO_3$ and $Fe_2^{3+}Fe^{3+}O_2BO_3$ [13-15] known as warwickites, ludwigites and morbergites correspondingly. The chemical formula which is deviated from ludwigites contains other structures, which is normally used to attain stability. The crystal structure based on Fe borates varies with

* Corresponding authors: sikander.physicst@gmail.com

compositions, microstructure and Fe-oxidation states. Biocompatible borates gain much attention in medical and biological compounds. The main compound containing one type of $Fe^{3+}(3d^5)$ spins is Fe_3BO_6, which is mostly used in catalysts, drugs, color pigments and biological tools [16-18].

In the early time of research, B_2O_3 was attained important preparations of glasses as scientific applications, and borate glasses was assumed to be good photo induced non linear optical aspects [19]. The transition metal oxides e.g (Fe_2BO_3) gained much attention in physical properties of glasses including electrical, optical, transport and magnetic properties. The physical and structral investigations of B_2O_3 doped with transition metals played key role in establishing the importance of these glasses including physical mechanisms based on such properties. The preparations of Fe_2BO_3 in bulk form was studied in solid state chemistry at high temperatures. This technique was made this single phase compound within functional characteristics. Shi et al [5]. investigated nanospherical Fe_2BO_3, formed by rheological phase reaction for lithium ion battery. Liu et al [6] studied Fe_3BO_6, by phase reaction solution process. Qi et al. [25] described Fe_3BO_5, for hydrothermal nanorod applications. This is only reason that no reports carried out on synthesis or other theoritical approaches in the formation of optoelectronic and tranport properties of this Fe_3BO_6.

Fe_2SiO_4 structural, electronic, elastic and thermodynamical properties have been investigated long time ago experimentally. It was analyzed that band gaps deviated from theoretically and experimentally for some spinel oxides. Orita et al. used first principles calculations for the investigation of electronic and structural properties of $InGaZnO_4$, and they deduced In-s states are responsible for the formation of the conduction band. Omura et al. observed that doping of indium improved the efficiency of the thin films, and they predict atomic concentrations of spinel compounds based on DFT pseudopotential approach. The electrical properties of n-channel semiconductors were also improved by point defect operations. F.Zerarga et al. used first principles on the spinel materials and computed calculated its opto-electronic properties by FPLAPW method in the energy range of 0-35 eV [20-24].

The aim of current research is to carry out DFT-based investigations of structral, optoelectronic, transport and magnetic properties of ferrite spinel oxides in pure and doped with Rh^{3+} with better accuracy. This technique helps us to investigate the properties which are not possible sometimes by expermentally. Now a days ab-initio calculations which are ofted called density functional theory (DFT) is important and essential tool of material science and condense matter physics. The whole computions were performed within framework of FP-LAPW method implemented in Wien 2k.

2. Structral Properties

The structral properties of Fe_3BO_6 and $Rh_{0.8}Fe_{0.92}BO_6$ materials have been performed volume optimizations using PBE GGA. The equilibrium lattice constants and bulk moduli are calculated by employing fitting Murnaghan equations of states to the total energy, which is implemented in Wien-2K. Since, optimization of materials key role in determining electronic, optical and transport of properties of investigated materials. The plots of optimizations reveals that Rh doped structure is more stable as compared to parental structures as indicated in figure 1b.

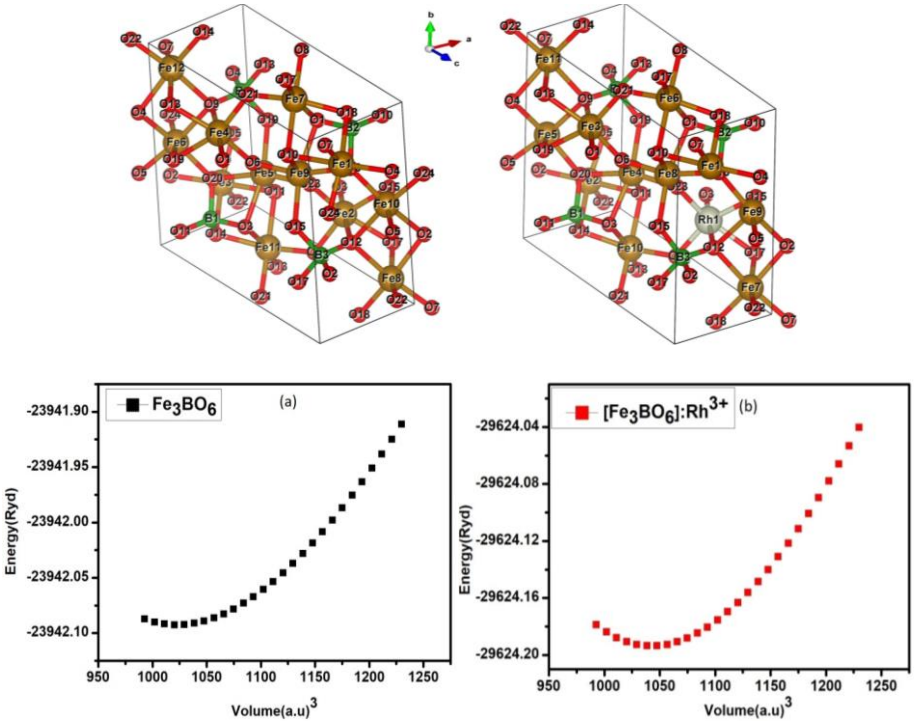

Fig. 1. Total energy versus volume calculated using several exchange–correlation functional for Fe_3BO_6 and $Rh_{0.8}Fe_{0.92}BO_6$ spinel oxides respectively.

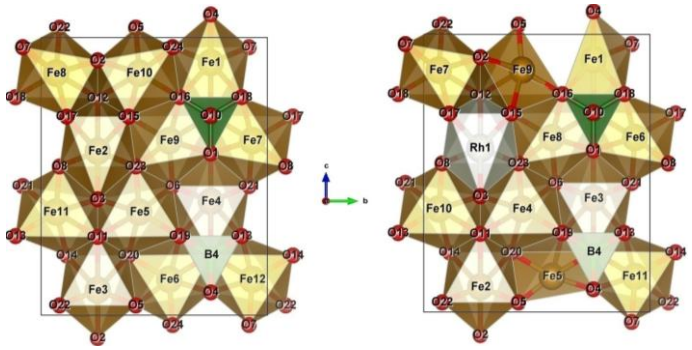

Fig. 2. Asymmetric unit structure of Fe_3BO_6 and $Rh_{0.8}Fe_{0.92}BO_6$ spinel oxides respectively.

3. Computational details

The spin polarized calculations based on first principles is used for electronic, optical and transport properties of spinel oxides family. The method used for this framework is full potential linearized augmented plane wave (FP-LAPW) implemented in simulation code Wien 2K [27], the exchange correlations functional (GGA+U)[28,29]. This scheme has been used for the computations of ground state properties of traced materials. This model based on the fact, whole crystal is splitted into non-overlapping spheres caused by interstitial region. Inside muffin tin (MT) spheres, a simple basis set is selected in term of spherical harmonics and plane waves are assumed in interstitial ranges. To avoid from the leakage electrons, we used semi-core states incorporated with local orbitals. For strongly correlated electronic system, the Hubbard value U=6.0 eV (U_{eff}=U-J) which adjust the Fe/Rh-d states in the electronic structure. The energy and charge convergence is achieved up to 10^{-4}Ry and 10^{-4}(a.u)^3 respectively. The muffin tin radius (R_{MT}) for each element is chosen such that no core electrons leakage occurred which ensured energy and charge convergence. The R_{MT} values for Fe, Rh, B and O are selected to be 1.80, 1.84, 1.20 and

1.39 respectively. These radii have been selected after analysis of different tests and different k-points to perform energy convergence. The angular momentum (l_{max}) inside atomic spheres is choose as 10 and plane wave cutoff $R_{MT}K_{Max}$=8 used for calculations.

The thermoelectric properties of spinel oxides were calculated by Post-DFT simulation code, based on Boltztmann transport theory called Boltztrap [29]. The electrical conductivity and Seebeck coefficient is computed given as

$$\sigma_{\alpha\beta(T;\mu)}=\frac{1}{\Omega}\int \sigma_{\alpha\beta}(\varepsilon)\left[-\frac{\partial f_\mu}{\partial \varepsilon}\right]d\varepsilon \quad (1)$$

$$S_{\alpha\beta(T;\mu)}=\frac{1}{eT\Omega\sigma_{\alpha\beta(\varepsilon)}}\int \sigma_{\alpha\beta}(\varepsilon)(\varepsilon-\mu)\left[-\frac{\partial f_\mu}{\partial \varepsilon}\right]d\varepsilon \quad (2)$$

In above equation, α and β are tensor indices, Ω is the unit cells volume, f is the fermi function and e is the electronic charge.

4. Results and discussion

4.1. Electronic and Magnetic observations

The physical properties of materials are mainly characterized by the understanding of electronic band structures. This may provide pleased nature of suitability of material in optoelectronic applications. The materials of direct band gap structure gained much attention in semiconducting industry while indirect plays weak role in the optical excitations phenomenon. The energy band structure is calculated for pure spinel Fe_3BO_6 and doped $Rh_{0.8}Fe_{0.92}BO_6$ is computed along high symmetry Brillioun zone points *(R, Γ, X, M, Γ)*, respectively shown in figure 3. The band structure is calculated by generalized gradient approximation plus Hubbard potential (GGA+U) implemented within framework of DFT for both spin channels of investigated materials. The portion above the fermi level is called conduction band while below its valence band, the electronic configuration of valence shell of Fe, Rh, B, and O are [Ar] $3d^6$ $4s^2$, [Kr] $4d^8$ $5s^1$, [He] $2s^2$ $2p^1$, and [He] $2s^2$ $3p^4$, respectively.

The energy band structure of pure and doped spinel oxides Fe_3BO_6 , $Rh_{0.8}Fe_{0.92}BO_6$ for both spin polarizations direction is shown in figure 3(a&b), respectively. The pure spinel Fe_3BO_6 shows direct band gaps (4.181 eV Up / 2.41 eV Dn), as valence band maxima (VBM) and conduction band minima (CBM) lies on *Γ*- point traced in figure 3a. Hence, its one channel (Up) exhibits insulated character and other (Dn) showing semiconducting. Doping effects the band structure and $Rh_{0.8}Fe_{0.92}BO_6$ shifts both direct polarizations in the semiconducting region [(2.59 eV (Up)/ 0.59 (Dn)], observed in figure 3b. The strong electron-hole mobility is occurred in both regions of VBM and CBM due to huge dispersions in K-space for both spinel oxides materials. The small shift in bandgaps after doping of Rh^{3+} in pure spinel caused paramagnetic character of compounds.

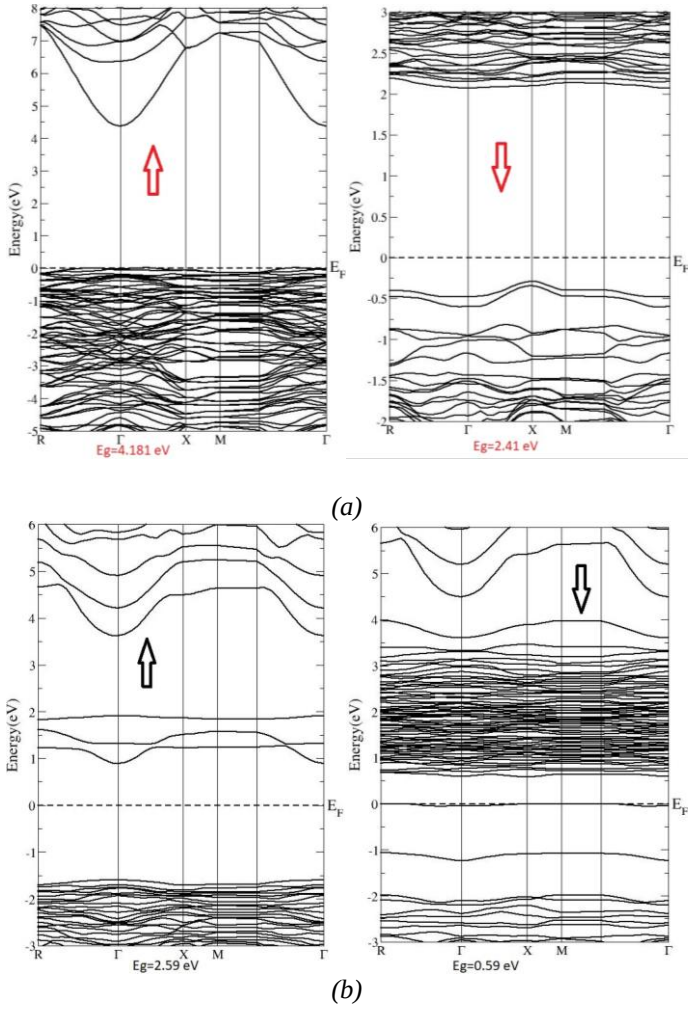

Fig. 3. Calculated energy band structure of spinel oxides (a) Fe_3BO_6 (b), $Rh_{0.8}Fe_{0.92}BO_6$ for both spins polarizations.

The atomic and orbital nature of electronic orbitals is attributed by density of states analysis, also used to clarify the electronic properties of spinel oxides as depicted in figure 4(a&b). The total and partial density of states (T/PDOS) is calculated within framework of (GGA+U) approach, explained contributions of different atomic orbitals in the band structure of both spin up and down channels of Fe_3BO_6, $Rh_{0.8}Fe_{0.92}BO_6$, respectively. Total density of states reveals that both valence and conduction bands mainly formed due to hybridizations of Fe, Rh and O orbitals. Usually, three regions are attributed first is the lower valence band (-10 eV to -6 eV), second is upper valence band (-6.0 eV to 0 eV) and last is the conduction band region (0 to 10 eV).

Partial density of states is directly related to contribution of different orbitals in the specified regions for both spin channels of investigated spinel oxides. It is observed from the figure 4, valence band is mainly originated by contributions of Fe, Rh-d and O-p orbitals for both spin polarizations while Fe, Rh, B(s,p) and O-s states minutely. The conduction band of investigated spinel oxides formed due to direct transitions of Fd, Rh- d states mainly indicated in figure 4. As our parental compounds up channel shows insulating nature, when we doped it with Rh its nature changed to semiconductor due to weakening the bonds. It is also noticed that Rh doping in pure spinel causes more complex band structure resulting reduced band gap due to interbank transitions between valence and conduction bands.

We have also computed the total and partial magnetic moments using GGA+U approximations. The total magnetic moment is the sum of partial magnetic moments and the interstitial sites occurred due to various atoms. The small contributions in the magnetic moment is

due to B and O atoms, may be neglected and major effect due to Fe and Rh atoms in the whole spinel oxides as indicated in table 1. As U is the Hubbard parameter, used only for strongly correlated system of Fe and Rh effects the ion localizations. The total magnetic moments for Fe within GGA+U approximations including the values of partial, interstitial and total magnetic moment are tabulated in table 1. The magnetic and electronic investigation shows that these materials have potential applications spintronics, optoelectronic and ferromagnetic materials.

Table 1. Spin Magnetic Moments of Mixed Charge Density.

:MMINT:	**MAGNETIC MOMENT IN INTERSTITIAL**	**=**	**3.36881**
:MMI001:	MAGNETIC MOMENT IN SPHERE 1	=	4.22143
:MMI002:	MAGNETIC MOMENT IN SPHERE 2	=	4.22149
:MMI003:	MAGNETIC MOMENT IN SPHERE 3	=	4.22142
:MMI004:	MAGNETIC MOMENT IN SPHERE 4	=	4.22149
:MMI005:	MAGNETIC MOMENT IN SPHERE 5	=	4.20623
:MMI006:	MAGNETIC MOMENT IN SPHERE 6	=	4.20546
:MMI007:	MAGNETIC MOMENT IN SPHERE 7	=	4.22779
:MMI008:	MAGNETIC MOMENT IN SPHERE 8	=	4.22977
:MMI009:	MAGNETIC MOMENT IN SPHERE 9	=	4.20622
:MMI010:	MAGNETIC MOMENT IN SPHERE 10	=	4.20546
:MMI011:	MAGNETIC MOMENT IN SPHERE 11	=	4.22779
:MMI012:	MAGNETIC MOMENT IN SPHERE 12	=	4.22976
:MMI013:	MAGNETIC MOMENT IN SPHERE 13	=	0.00140
:MMI014:	MAGNETIC MOMENT IN SPHERE 14	=	0.00140
:MMI015:	MAGNETIC MOMENT IN SPHERE 15	=	0.00141
:MMI016:	MAGNETIC MOMENT IN SPHERE 16	=	0.00141
:MMI017:	MAGNETIC MOMENT IN SPHERE 17	=	0.18243
:MMI018:	MAGNETIC MOMENT IN SPHERE 18	=	0.18419
:MMI019:	MAGNETIC MOMENT IN SPHERE 19	=	0.18244
:MMI020:	MAGNETIC MOMENT IN SPHERE 20	=	0.18420
:MMI021:	MAGNETIC MOMENT IN SPHERE 21	=	0.33076
:MMI022:	MAGNETIC MOMENT IN SPHERE 22	=	0.32056
:MMI023:	MAGNETIC MOMENT IN SPHERE 23	=	0.25320
:MMI024:	MAGNETIC MOMENT IN SPHERE 24	=	0.25840
:MMI025:	MAGNETIC MOMENT IN SPHERE 25	=	0.15784
:MMI026:	MAGNETIC MOMENT IN SPHERE 26	=	0.15813
:MMI027:	MAGNETIC MOMENT IN SPHERE 27	=	0.15813
:MMI028:	MAGNETIC MOMENT IN SPHERE 28	=	0.15783
:MMI029:	MAGNETIC MOMENT IN SPHERE 29	=	0.17033
:MMI030:	MAGNETIC MOMENT IN SPHERE 30	=	0.17025
:MMI031:	MAGNETIC MOMENT IN SPHERE 31	=	0.17922
:MMI032:	MAGNETIC MOMENT IN SPHERE 32	=	0.17925
:MMI033:	MAGNETIC MOMENT IN SPHERE 33	=	0.17033
:MMI034:	MAGNETIC MOMENT IN SPHERE 34	=	0.17025
:MMI035:	MAGNETIC MOMENT IN SPHERE 35	=	0.17921
:MMI036:	MAGNETIC MOMENT IN SPHERE 36	=	0.17927
:MMI037:	MAGNETIC MOMENT IN SPHERE 37	=	0.25841
:MMI038:	MAGNETIC MOMENT IN SPHERE 38	=	0.25319
:MMI039:	MAGNETIC MOMENT IN SPHERE 39	=	0.32056
:MMI040:	MAGNETIC MOMENT IN SPHERE 40	=	0.33075
:MMTOT:	**SPIN MAGNETIC MOMENT IN CELL**	**=**	**59.08787**

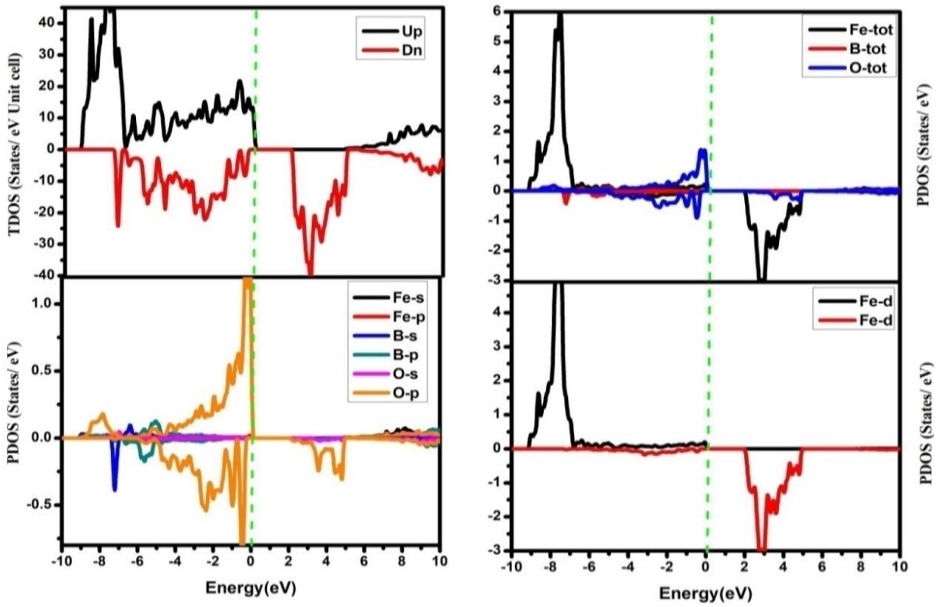

(a)

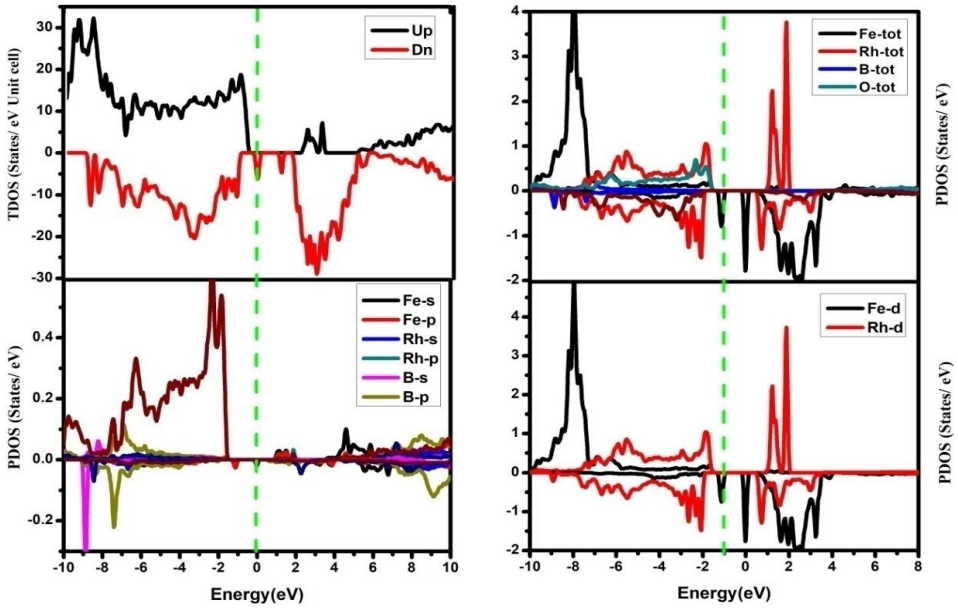

(b)

Fig. 4 Calculated total densities of states (states/eV unit cell) for (a) Fe_3BO_6 (b), $Rh_{0.8}Fe_{0.92}BO_6$ for both spins polarizations.

4.2. Optical Properties

The optical features of semiconducting materials play crucial role in optoelectronic industry. The understanding of optical properties is essential for its role in applications as photonic devices. The whole optical properties of investigated materials are based on complex dielectric functions$\varepsilon(\omega)$, is given as [30]

$$\varepsilon(\omega) = \varepsilon_1(\omega) + i\varepsilon_2(\omega) \tag{3}$$

Here, first and second term exhibits the real and imaginary parts of complex dielectric function, respectively. The optical dispersions like refractive index$n(\omega)$, optical absorption

coefficient α(ω), normal incident reflectivity R(ω), and energy loss function L (ω) semiconducting materials can be calculated from real and imaginary parts of complex dielectric function.

The real part (dispersive part) $\varepsilon_1(\omega)$, is calculated by Kramers Kroning relations (KKR) given by this relations below

$$\varepsilon_1(\omega) = 1+\frac{2}{\pi}\, M \int_0^{\infty} \frac{\omega^{/}\, \varepsilon_2(\omega^{/})}{\omega^{/2}-\omega^2}\, d\omega^{/} \tag{4}$$

Figure 4 exhibits the dispersive part of dielectric function in the range of 0-14 eV for both spin channels. The static value of dielectric function for parent and doped materials are tabulated in table 2.

The real part of dielectric function is directly connected to polarizability of electromagnetic spectra, which are mainly formed due to interband transitions as indicated in figure 5. The density of states used to remove the deficiencies by employing selection rule in the dispersive part of investigated materials. Figure 5 exhibits the changes in the dispersive part with photons energy; the parent compound shows dispersion around 3 eV and doped showing around 2 eV for both spin channels. On further increase in the energy, few bumps are observed due to interband transitions and after reaching its maximum, it starts flattens as indicated in figure 5. The positive nature of real part of dielectric function is pleased as semiconducting materials, while negative peaks are termed as reflection of incident photons. The static value of real dielectric function is 1.6, 3.3 (Up/Dn) and 1.8, 2.9 (Up/Dn) for Fe_3BO_6, $Rh_{0.8}Fe_{0.92}BO_6$, respectively.

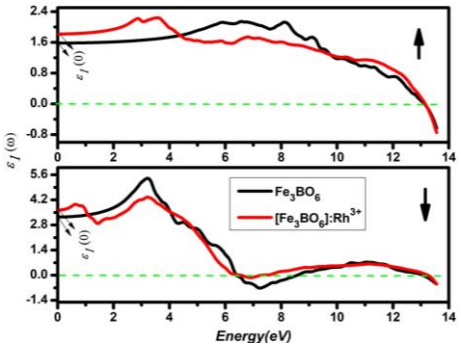

Fig. 5. Variation of dispersive part of dielectric function with energy for (a) Fe_3BO_6 (b), $Rh_{0.8}Fe_{0.92}BO_6$ for both spins polarizations.

The phenomenon of jumping of electrons from the valence band to conduction bands is named as absorption coefficient, which occurred due to absorption of photons. Figure 6 shows the threshold value of imaginary part of dielectric function appear at 5.0 eV/2.3 eV (Up/Dn) and 2.8 eV/0.5 eV (Up/Dn) for Fe_3BO_6, $Rh_{0.8}Fe_{0.92}BO_6$, respectively. The small peaks in the $\varepsilon_2(\omega)$ traced due to interband transitions between VBM and CBM as shown in figure 6, Direct transitions are responsible while in contributions of mainly peaks evolved in absorptive coefficient. It is observed from mentioned figure, the maximum absorption for parent compound occurred at 9 eV/5 eV (Up/Dn) and for doped material it's in ultraviolet region. The main peaks in the spectra are due to conduction band (unoccupied states) and valence band (occupied states). The imaginary part of complex dielectric function is derived from KKR relations given as

$$\varepsilon_2(\omega) = \frac{Ve^2}{2\pi\hbar m^2\omega^2} \int d^3\, k \sum_{nn'} \left|\langle \vec{k}n \left| p \right| \vec{k}n' \rangle\right|^2 f(\vec{k}n)\left[1 - f(\vec{k}n')\right]\delta(E_{\vec{k}n} - E_{\vec{k}n'} - \hbar\omega) \tag{5}$$

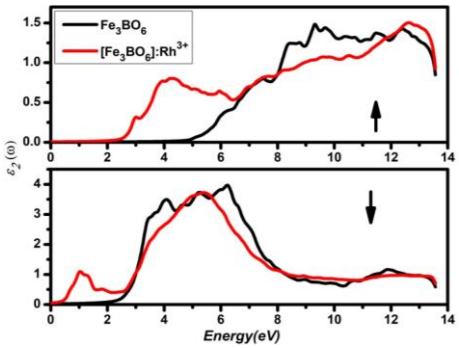

Fig. 5. Variation of absorptive part of dielectric function with energy for (a) Fe_3BO_6 (b), $Rh_{0.8}Fe_{0.92}BO_6$ for both spins polarizations.

The energy loss function [31] (loss of fast electrons) computed by photons energy 0-14 eV is shown in figure 7. The behavior of this loss is seen isotropic in the lower energy range while anisotropy observed in the UV region. The Plasmon excitations occurred where the loss contains maximum value, due to VBM and CBM. At lower energy region, minute loss is observed and reached to maximum at higher energy range for both investigated materials. It is also linked to reflectivity, so as abrupt reduction in the spectra caused from the energy loss function.

Another important optical parameter is the reflectivity$R(\omega)$, which has inverse relations with energy loss function shown in figure 7 b. The limit of zero frequency is occurred at 0.02,0.9 (Up/Dn) and 0.05, 0.15 (Up/Dn), respectively for Fe_3BO_6, $Rh_{0.8}Fe_{0.92}BO_6$. Hence, huge reflection occurred in UV regions as compared to IR and visible indicated in figure 7b. Some fluctuations are assumed in figure due to interband transitions, its ration increased on doping with Rh^{3+}. It is noticed from mentioned figure, 40 % reflectivity seen due to Fe/Rh-d orbitals. The peaks where dispersive part is assumed to be negative are due to 4, 6, 7 and 13 eV in reflection spectra.

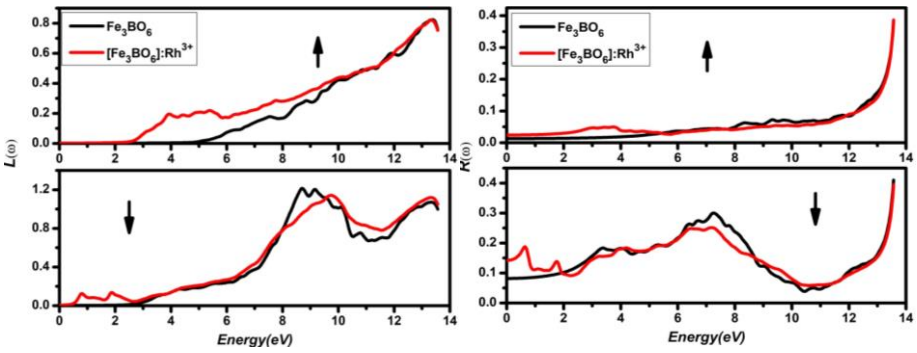

(a) *(b)*

Fig. 7. Variation of energy loss function and reflectivity with radiation energy for (a) Fe_3BO_6 (b), $Rh_{0.8}Fe_{0.92}BO_6$ for both spins polarizations.

The atomic interactions plays wide role in the optical properties caused refraction phenomenon $n(\omega)$ at micro level, it's directly connected to real part of dielectric function expressed as [32]

$$n(\omega) = \left[\frac{\sqrt{\varepsilon_1^2(\omega)+\varepsilon_2^2(\omega)}}{2} + \frac{\varepsilon_1(\omega)}{2}\right]^{1/2} \quad (6)$$

The static value of refractive index is basically square root of dispersive part of dielectric functions given by these relations

$$n(0) = \sqrt{\varepsilon_1(0)} \tag{7}$$

Figure 8 expressed the variations of refractive index in which role of phonons are assumed to be neglected in order to achieve the dielectric screening. When the energy of photon increased, $n(\omega)$ also gets some fluctuations and decreased in UV region for both parent and doped compound. The static value of refractive index 1.2, 1.6 ((Up/Dn) and 1.4, 2.3 ((Up/Dn) for Fe_3BO_6 and $Rh_{0.8}Fe_{0.92}BO_6$, respectively. The refractive index of crystals is connected to electronic polarizability of local fields and ions interior the crystals. The peaks of refractive index are reached to their maxima around 2 eV to 4.5 eV for both investigated materials. Hence, these materials are non-transparent in the IR and visible region but transparent in UV region.

The extinction coefficient is basically penetrations of light in material formed by relation as combination of real part of refractive index $n(\omega)$ and extinction coefficient $k(\omega)$[33] basically provide a complex refractive index.

$$N(\omega) = n(\omega) + ik(\omega) = [\varepsilon_1 + i\varepsilon_2]^{1/2} \tag{8}$$

$$k(\omega) = \left[\frac{\sqrt{\varepsilon_1^2(\omega)+\varepsilon_2^2(\omega)}}{2} - \frac{\varepsilon_1(\omega)}{2}\right]^{\frac{1}{2}} \tag{9}$$

The imaginary part of dielectric function is similar to extinction coefficient, which plays key role in absorption spectra for both spin channels of Fe_3BO_6 and $Rh_{0.8}Fe_{0.92}BO_6$, respectively. Figure 8 exhibits the absorption spectra associated interband transitions, which are pleased in the UV range, and it goes on decreasing in the range of 14 eV.

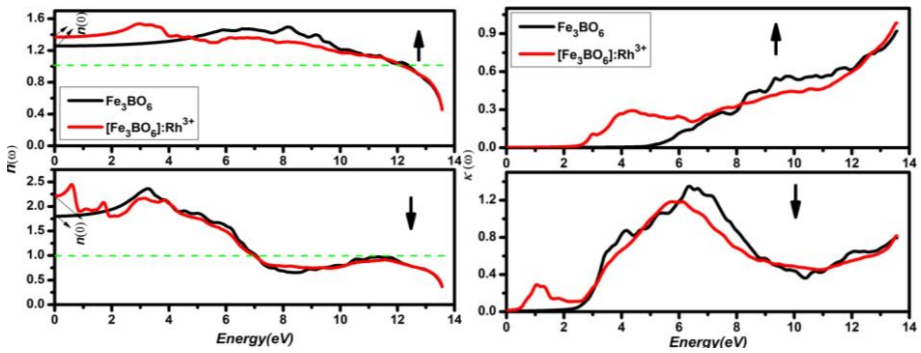

Fig. 8. Refractive index and extinction coefficient for (a) Fe_3BO_6 (b), $Rh_{0.8}Fe_{0.92}BO_6$ for both spins polarizations.

The absorption spectra [34] associated with parent and doped materials depends on nature of materials, as shown in figure 9 for both channels of spin polarizations of Fe_3BO_6 and $Rh_{0.8}Fe_{0.92}BO_6$, respectively. This property of materials play key role in designing and fabrication of optical devices for both spin up and down spectra. The relation used to investigate absorption spectra is related to complex dielectric function given as

$$\alpha(\omega) = \sqrt{2}\omega\left[\{\varepsilon_1^2(\omega) + \varepsilon_2^2(\omega)\}^{1/2} - \varepsilon_1(\omega)\right]^{1/2} \tag{10}$$

At low energy range, no absorption occurred and material shows transparent nature due to forbidden bands, observed in figure 10. Both investigated materials shown good absorption in the UV region. $\alpha(\omega)$ Connected to optical band gap of compounds which are 5.5 eV/3.0 eV (Up/Dn) and 3.0 eV/0.5 eV(Up/Dn) Fe_3BO_6 and $Rh_{0.8}Fe_{0.92}BO_6$, respectively.

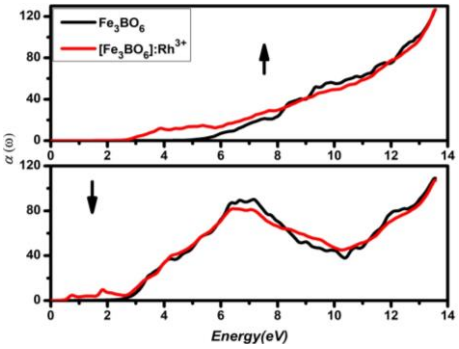

Fig. 9. Variation of absorption coefficnient (a) Fe_3BO_6 (b), $Rh_{0.8}Fe_{0.92}BO_6$ for both spins polarizations.

Table 2. Calculated optical dispersion parameters of Fe_3BO_6 and $Rh_{0.8}Fe_{0.92}BO_6$.

Compounds	E_g (eV)	$\varepsilon_1(0)$	*n(0)*	α(ω)	κ (ω)	L (ω)	*R(0)*
Fe_3BO_6	4.181 Up 2.41 Dn	1.6 Up 2.9 Dn	1.2 Up 1.75 Dn	5.0 Up 2.5 Dn	0.8 Up 1.3 Dn	0.8 Up 1.1 Dn	0.01 Up 0.9 Dn
$Rh_{0.8}Fe_{0.92}BO_6$	2.59 Up 0.59 Dn	1.8 Up 3.0 Dn	1.5 Up 2.3 Dn	3.0 Up 0.7 Dn	0.99 Up 1.09 Dn	0.8 Up 1.2 Dn	0.03 Up 0.15 n

5. Thermoelectric Properties

Thermal energy sources play important role in the production of electrical energy which are mainly used in thermoelectric applications. The researchers have been studied thermoelectric properties extensively e,g detectors and computer cooling devices. The new spinel compound Fe_3BO_6 and $Rh_{0.8}Fe_{0.92}BO_6$ could be used as thermoelectric materials because of suitability of transport parameters with variations in the temperature. The simulations code based on rigid band approximations used for the investigation of thermoelectric properties of materials is Boltztrap.

The thermoelectric property based on band structure, is electrical conductivity (σ) which is flow of free charge carriers notable parameter computed in range 0-850 K exhibited in figure 10. The thermally excited electrons from the CB show the linear response 0.0×10^{17} $(\Omega\ m\ s)^{-1}$ to 2.0×10^{17} $(\Omega\ m\ s)^{-1}$ and 1.18×10^{18} $(\Omega\ m\ s)^{-1}$ to 6.0×10^{17} $(\Omega\ m\ s)^{-1}$ for Fe_3BO_6 and $Rh_{0.8}Fe_{0.92}BO_6$, respectively against temperature range of 50 to 800 K, as shown in figure 11 (a). Figure exhibits that doped material gain higher value of electrical conductivity as compared to parent compound.

The second parameter is Seebeck coefficient [34], is the ratio between differences of voltage to temperature contains prestigious effect to determine the efficiency of thermocouples. Figure 11 indicate the computed seebeck coefficient for Fe_3BO_6 and $Rh_{0.8}Fe_{0.92}BO_6$, both spin channels. Parent compound Fe_3BO_6, represents p-type nature and doped $Rh_{0.8}Fe_{0.92}BO_6$ exhibits n-type character as plotted in mentioned figure. It is also seen that parent compound has highest value at low temperature and on increasing T, its decreased linearly.

Thermal conductivity [35] is the key feature to investigate the heat conduction, semiconducting materials contains phonons as majority carriers. Figure 12 shows the thermal conductivity of investigated materials, both materials shows lower value in the lower energy range and linear increased is seen at higher temperatures. At 800 K, the highest value of thermal conductivity is for Fe_3BO_6 and $Rh_{0.8}Fe_{0.92}BO_6$, $1.18x10^{13}$ W/mKs and $0.5x10^{12}$ W/mKs,

respectively. The material Fe_3BO_6 exhibits unparalleled character as compared to dope $Rh_{0.8}Fe_{0.92}BO_6$.

As we are interested to attain good efficiency of investigated compounds, Power factor [36,37]is parameter which is calculated and plotted in figure 13. It is analyzed from plot that high P.F is attained at 800 K, 2.454 x 10^{10} W/mk^{2}s highest value for parental compound. So, parental compound Fe_3BO_6 pleased to be good applications in waste heat management morphology as that of doped Rh compound, indicated in figure 13. Figure of merit (ZT) [38] is another thermoelectric parameter to measure effectiveness of materials. The material is said to be more effective if it has high value of ZT. Figure 14 exhibits that Fe_3BO_6 achieved ZT value around unity and showed stability up to high temperature. The variations of ZT value with temperature range is tabulated in table 3.

Table 3. Calculated transport parameters of Fe_3BO_6 and $Rh_{0.8}Fe_{0.92}BO_6$.

Compounds	**(μV/K)**		**(W/Kms)**		**(1/cm)**		**(W/mK^{2}s)**		**(ZT)**	
	50K	800K	50K	800K	50K	800K	50K	800K	50K	800K
Fe_3BO_6	20	30	0.01×10^{13}	1.18×10^{13}	0.01×10^{17}	2.0×10^{17}	0.1×10^{9}	2.0×10^{10}	0.9	1.0
$Rh_{0.8}Fe_{0.92}BO_6$	2500	500	0.2×10^{12}	5×10^{12}	0.0×10^{14}	1.18×10^{18}	0.12×10^{9}	0.28×10^{9}	0.1	0.2

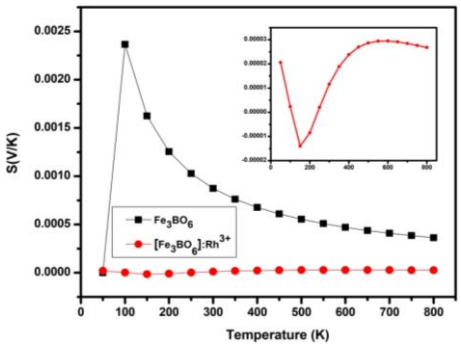

Fig. 10. Seebeck Coefficent for spinel oxides Fe_3BO_6 and $Rh_{0.8}Fe_{0.92}BO_6$ compounds.

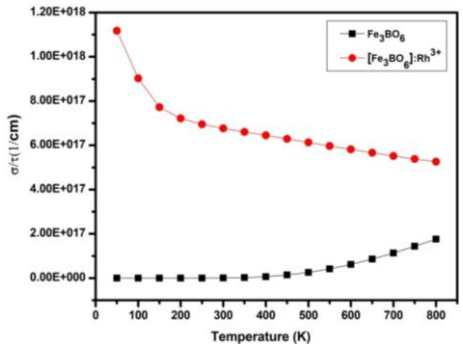

Fig. 11. Electrical conductivity of spinel oxides Fe_3BO_6 and $Rh_{0.8}Fe_{0.92}BO_6$ compounds.

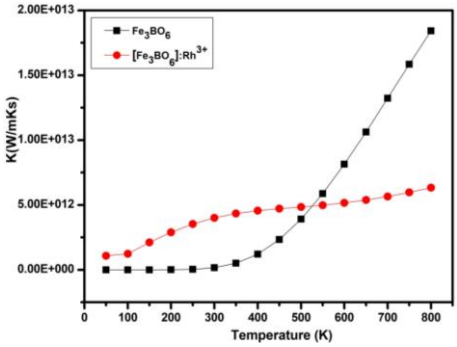

Fig. 12.Thermal conductivity of spinel oxides Fe_3BO_6 and $Rh_{0.8}Fe_{0.92}BO_6$ compounds.

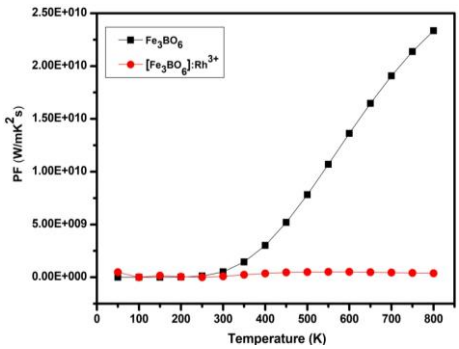

Fig. 12. Power factor of spinel oxides Fe_3BO_6 and $Rh_{0.8}Fe_{0.92}BO_6$ compounds.

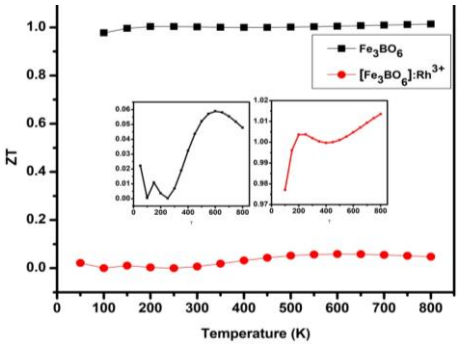

Fig. 13. Figure of merit of spinel oxides Fe_3BO_6 and $Rh_{0.8}Fe_{0.92}BO_6$ compounds

6. Conclusions

In summary, we have computed structural, electronic, optical, magnetic and thermoelectric properties of spinel oxides using DFT, based on first principles calculations performed within framework of FP-LAPW method as implemented in Wien 2k simulation package. As Fe and Rh d states unfilled, so we used GGA+U approximation, here U is Hubbard parameter whose value is set at 7.0 eV for both spin channels of Fe_3BO_6 and $Rh_{0.8}Fe_{0.92}BO_6$.

The electronic calculation reveals that both compounds showed direct nature of bands lies in the semiconducting range, as valence band maxima and conduction band minima lies on the gamma point. The total and partial density of states assumed the contribution of Fe/Rh-d orbitals observed mainly for interband transitions for both investigated spinel's. . The optical dispersion of complex dielectric function$\varepsilon(\omega)$, energy loss function $L(\omega)$, refractive index $n(\omega)$, extinction coefficient $k(\omega)$, reflectivity $R(\omega)$, and optical conductivity $\sigma(\omega)$ were observed deeply in the

range of 0-14 eV. These materials revealed good anisotropy in the visible and UV range of energy; hence they can be good optical materials in the semiconducting industry. The thermoelectric properties calculated using semi classical theory by Boltzmann code, such as the electrical conductivity (σ/τ), electronic thermal conductivity (κ_e/τ), and Seebeck coefficient (S), Power factor (P.F) and figure of merit (ZT).

The effective masses of electrons and holes were also calculated by fitting the parabolic function, which observed the point of inflection occurred where the nature of materials changed from direct to indirect at 6.9. The results of P.F and ZT values lie in the desirable range for the effectiveness of spinel oxides as thermoelectric applications.

Acknowledgment

The author (R. Neffati) extends his appreciation to the Deanship of Scientific Research at King Khalid University, Saudi Arabia for funding this work through Research Groups Program under grant number (R.G.P.2/170/42).

References

[1] M. Mir, R. B. Guimarães, J. C. Fernandes, M. A. Continentino, A. C. Doriguetto, Y. P. Mascarenhas, J. Ellena, E. E. Castellano, R. S. Freitas, L. Ghivelder, Phys. Rev. Lett. **87**, 147201-1-4 (2001).
[2] J. C. Fernandes, R. B. Guimarães, M. A. Continentino, E. C. Ziemath, L. Walmsley, M. Monteverde, M. N. Regueiro, J. L. Tholence, J. Dumas. Phys. Rev. B **72**, 075133-1-5 (2005).
[3] S. Shimomura, S. Nakamura, N. Ikeda, E. Kaneko, K. Kato, K. Kohn, J. Magn. Magn. Mater. **310**, 793 (2007).
[4] D. C. Freitas, M. A. Continentino, R. B. Guimarães, J. C. Fernandes, J. Ellena, L. Ghivelder, Phys. Rev. B **77**, 184422-1-8 (2008).
[5] X. Shi, C. Chang, J. Xiang, Y. Xiao, L. Yuan, J. Sun, J. Solid State Chem. **181**, 2231 (2008).
[6] Y. Liu, S. Peng, Y. Ding, C. Rong, J. Kim, J. P. Liu, Z. L. Wang, S. Sun, Adv. Func. Mater. **19**, 3146 (2009).
[7] T. Kawano, H. Morito, T. Yamada, T. Onuma, S. F. Chichibu, H. Yamane, J. Solid State Chem. **182**, 2004 (2009).
[8] S. K. Das, M. Nandi, S. Giri, A. Bhaumik, Microporous Mesoporous Mater. **117**, 362 (2009).
[9] R. Diehl, Solid State Commun. **17**, 743 (1975).
[10] R. Diehl, G. Brandt, Acta Crystallogr. B **31**, 1662 (1975).
[11] J. P. Attfield, J. F. Clarke, D. A. Perkins, Physica B **180**, 581 (1992).
[12] J. S. Swinnea, H. Steinfink, Am. Mineral. **68**, 827 (1983).
[13] J. S. Knyrima, H. Huppertz, J. Solid State Chem. **181**, 2092 (2008).
[14] T. A. Kravchuk, Y. D. Lazebnik, Russ. J. Phys. Chem. **12**, 21 (1967).
[15] I. M. Rumanova, E. A. Genkina, N. V. Belov, Latvian SSR Academy of Sciences Chemistry Series **5**, 571 (1981).
[16] S. Block, G. Burley, A. Perloff, R. D. Mason Jr., Journal of research of the National Bureau of Standards **62**, 95 (1959).
[17] L. A. Bauer, N. S. Birenbaum, G. J. Meyer, J. Mater. Chem. **14**, 517 (2004).
[18] M. P. Chung, (Ed.), Handbook on borates: chemistry, production and applications, Nova Publishers, Huntington, New York, USA, 2009.
[19] I. V. Kityk, W. Imiolek, A. Majchrowski, E. Michalski, Opt. Commun. **219**, 421 (2003).
[20] P. Pascuta, R. Lungu, I. Ardelean, J. Mater. Sci: Mater. Electron. **21**, 548 (2010).
[21] S. Ram, K. Kumari, R. K. Kotnala, Trans. Ind. Ceram. Soc. **69**(3), 165 (2010).
[22] K. Kumari, K. K. Bhargav, N. Kumar, S. Ram, R. K. Kotnala, Phys. Status Solidi A **208**, 2130 (2011).
[23] K. Kumari, S. Ram, R. K. Kotnala, Philos. Mag. Lett. **91**, 498 (2011).

[24] K. Kumari, S. Ram, R. K. Kotnala, Mater. Chem. Phys. **129**, 1020 (2011).
[25] H. Qi, Q. Chen, Chemistry Letters **37**, 752 (2008).
[26] J. Wallot, P. Reynders, J. Rödel, J. Am. Ceram. Soc. **91**, 3856 (2008).
[27] V. G. Tyuterev, N. Vast, Computational materials science **38**(2), 350 (2006).
[28] P. G. Etchegoin, E. C. Le Ru, M. Meyer, The Journal of chemical physics **125**(16), 164705 (2006).
[29] O. Sato, Y. Tanaka, M. Kobayashi, A. Hasegawa, Physical Review B **48**(3), 1947 (1993).
[30] A. Weidlich, A. Wilkie, Anomalous dispersion in predictive rendering, In Computer Graphics Forum **28**(4), 1065 (2009), Oxford, UK: Blackwell Publishing Ltd.
[31] A. Rahmati, M. Ghoohestani, H. Badehian, M. Baizaee, Materials Research **17**(2), 303 (2014).
[32] P. Wilcox, M. Lowe, P. Cawley, NDT & E International **34**(1), 1 (2001).
[33] S. Kumar, S. S. Parashari, S. Auluck, Phys. Stat. Sol. B **246**, 2294 (2009).
[34] A. R. Chandra, V. Jain, N. Lakshmi et al., Journal of Alloys and Compounds. **748**, 298 (2018).
[35] S. Buller, (2012). Phasenwechselmedien-Einfluss der chemischen Substitution auf die Eigenschaften von Speichermedien und Thermoelektrika (Doctoral dissertation).
[36] Chwan K. Chiang, C. R. Fincher Jr., Yung W. Park, Alan J. Heeger, Hideki Shirakawa, Edwin J. Louis, Shek C. Gau, Alan G. MacDiarmid, Physical review letters **39**(17), 1098 (1977).
[37] W. S. Williams, Jom, **50**(6), 62 (1998).
[38] C. Cho, K. L. Wallace, P. Tzeng, J. H. Hsu, C. Yu, J. C. Grunlan, Advanced Energy Materials **6**(7), 1502168 (2016).